Two azimuthally separated regions of cusp ion injection observed via energetic neutral atoms

M. Abe,[1] S. Taguchi,[1,2] M. R. Collier,[3] and T. E. Moore[3]

Received 22 April 2011; revised 1 August 2011; accepted 3 August 2011; published 20 October 2011.

[1] The low-energy neutral atom (LENA) imager on the IMAGE spacecraft can detect energetic neutral atoms produced by ion injection into the cusp through a charge exchange with the Earth's hydrogen exosphere. We examined the occurrence of the LENA cusp signal during positive IMF B_Z in terms of the arrival direction and the IMF clock angle θ_{CA}. Results of statistical analyses show that the occurrence frequency is high on the postnoon side when θ_{CA} is between ~20° and ~50°. This is ascribed to ion injection caused by cusp reconnection typical of positive IMF B_Z. Our results also show that there is another situation of high occurrence frequency, which can be identified with θ_{CA} of ~30° to ~80°. When θ_{CA} is relatively large (60°–80°), occurrence frequencies are high at relatively low latitudes over a wide extent spanning both prenoon and postnoon sectors. This feature suggests that the ion injection is caused by reconnection at the dayside magnetopause. Its postnoon side boundary shifts toward the prenoon as θ_{CA} decreases. When θ_{CA} is less than ~50°, the high occurrence frequency exists well inside the prenoon sector, which is azimuthally separated from the postnoon region ascribed to cusp reconnection. The prenoon region, which is thought due to ion injection caused by dayside reconnection, may explain the recent report that proton aurora brightening occurs in the unanticipated prenoon sector of the northern high-latitude ionosphere for IMF $B_Y > 0$ and $B_Z > 0$.

Citation: Abe, M., S. Taguchi, M. R. Collier, and T. E. Moore (2011), Two azimuthally separated regions of cusp ion injection observed via energetic neutral atoms, *J. Geophys. Res.*, *116*, A10225, doi:10.1029/2011JA016778.

1. Introduction

[2] When the interplanetary magnetic field (IMF) has a northward component, reconnection can occur on the magnetopause poleward of the cusp. In the context of the antiparallel reconnection hypothesis, the manner in which this reconnection site is shifted azimuthally is related to the east-west component (i.e., the *Y*-component) of the IMF. When this *Y*-component (IMF B_Y) is positive, the reconnection site occurs in the northern postnoon sector (or southern prenoon sector). The site shifts to the northern prenoon sector (or southern postnoon sector) when IMF B_Y is negative [e.g., *Crooker*, 1979; *Luhmann et al.*, 1984].

[3] While spacecraft observations in the vicinity of the reconnection site on the magnetopause have provided direct evidence of the existence of this cusp reconnection [e.g., *Kessel et al.*, 1996; *Avanov et al.*, 2001; *Lavraud et al.*, 2002, 2005; *Phan et al.*, 2003], the IMF B_Y dependence of the reconnection site has been most clearly demonstrated through the observations made at ionospheric height. The cusp and polar cap ionosphere, which is connected to the region near the reconnection site through the Earth's magnetic field lines, manifests a well-defined region of sunward convection when the IMF has a northward component [e.g., *Maezawa*, 1976; *Burke et al.*, 1979; *Reiff*, 1982; *Matsuoka et al.*, 1996]. This sunward convection is driven by the cusp reconnection and thus has characteristics that are consistent with the B_Y-dependent location of the cusp reconnection [e.g., *Reiff and Burch*, 1985; *Heelis et al.*, 1986; *Knipp et al.*, 1993; *Taguchi and Hoffman*, 1996; *Eriksson et al.*, 2002], which provides evidence for the theory that antiparallel reconnection is dominantly operative for northward IMF.

[4] Reconnection injects particles from the reconnection site, and those particles precipitate into the cusp ionosphere along the Earth's magnetic field lines. Recent techniques for observing the precipitating particles by remote sensing from spacecraft are also effective for identifying the IMF-dependent feature of the cusp reconnection site. Using data from the imager on the Polar spacecraft [*Torr et al.*, 1995], *Milan et al.* [2000] have shown that during a positive IMF B_Z the auroral emission caused by the precipitating electrons is located in the prenoon or postnoon sector of the northern hemisphere for $B_Y < 0$ or $B_Y > 0$, respectively. *Frey et al.* [2002] showed that the location of the proton injection has a similar tendency, by examining proton auroral spots in the dayside ionosphere with the spectrographic imager SI-12 of

[1]Department of Communication Engineering and Informatics, University of Electro-Communications, Tokyo, Japan.
[2]Center for Space Science and Radio Engineering, University of Electro-Communications, Tokyo, Japan.
[3]NASA Goddard Space Flight Center, Greenbelt, Maryland, USA.

Copyright 2011 by the American Geophysical Union.
0148-0227/11/2011JA016778

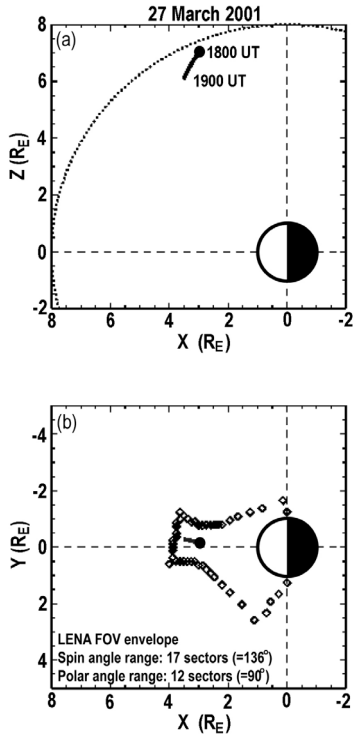

Figure 1. Position of IMAGE in (a) $X_{GSM}Z_{GSM}$ and (b) $X_{GSM}Y_{GSM}$ planes for 27 March 2001, 1800–1900 UT. The solid circle indicates the location of the spacecraft at 1800 UT. The dotted curve in Figure 1a shows the radial distance of 8 R_E from the center of the Earth. The region surrounded with diamonds in Figure 1b indicates a 136° (=17 spin angle sectors) × 90° (=12 polar angle sectors) LENA's FOV at 1842 UT, which is mapped on the sphere with a radius of 8 R_E. In Figure 1b the projected FOV is viewed from outside the 8 R_E sphere.

the far-ultraviolet instrument (FUV) on the IMAGE spacecraft [*Mende et al.*, 2000].

[5] However, a more recent study has shown that a different approach to event selection from the IMAGE SI-12 data leads to a different result. *Bobra et al.* [2004] first selected intervals from the IMAGE database to satisfy solar wind criteria, and then they examined the SI-12 images. Their result for $B_Y > 0$ and $B_Z > 0$ shows that the ion injection site has no strong preference for either side of local noon, which contradicts the earlier result indicating that the cusp ion injection occurs predominantly in the postnoon sector for that IMF condition. *Bobra et al.* [2004] implied that the prenoon injection is possibly caused by more intense ion precipitation due to ion drift paths within the magnetosphere preferentially intersecting the magnetopause in the prenoon sector. Nevertheless, further studies are needed for a definitive understanding of the ion injection in the unanticipated prenoon sector for positive B_Y [*Frey*, 2007].

[6] In this study, we identify the characteristics of the ion injection in the daytime sector for positive B_Y during northward IMF by using a remote sensing approach with energetic neutral atoms detected by the low-energy neutral atom (LENA) imager [*Moore et al.*, 2000, 2001] on the IMAGE spacecraft. The LENA imager is capable of detecting not only energetic neutral atom (ENA) emissions produced by ion injection into the cusp through a charge exchange with the Earth's hydrogen exosphere [*Taguchi et al.*, 2004a, 2004b, 2005, 2006, 2009a, 2009b; *Murata et al.*, 2007; *Suzuki et al.*, 2008] but also ENA emissions from the magnetosheath flow near the subsolar magnetopause [*Collier et al.*, 2001a, 2001b, 2005; *Moore et al.*, 2003; *Fok et al.*, 2003; *Taguchi et al.*, 2004a; *Hosokawa et al.*, 2008]. It has been shown that magnetosheath imaging can be done in soft X-rays [*Collier et al.*, 2010]. Observations made by a recently launched spacecraft, the Interstellar Boundary Explorer [*McComas et al.*, 2009], have also shown that strong ENA emissions are present in the magnetosheath and the cusp [*Fuselier et al.*, 2010; *Petrinec et al.*, 2011].

[7] In contrast to previous LENA studies, which were based on data obtained continuously for several hours during one day, we first conducted a statistical analysis of LENA signals observed on several days by taking into account the difference in the field of view (FOV) of the LENA imager. Results of this analysis show that the occurrence frequency of the cusp ion injection, which is deduced from the LENA signal, is high in the azimuthally separated prenoon and postnoon sectors of the northern magnetosphere for clock angles θ_{CA} of ~30° to ~50°. Our result also shows that the prenoon region, which occurs in the sector unfavorable for antiparallel reconnection, tends to extend azimuthally as θ_{CA} increases. From these characteristics, we consider the source of ion injection for either region, and we explain why proton aurora brightening can occur in the unanticipated prenoon sector of the northern high-latitude ionosphere for $B_Y > 0$ and $B_Z > 0$, as was found by *Bobra et al.* [2004].

2. Importance of LENA Imager FOV to Cusp Ion Monitoring

[8] The LENA imager on the IMAGE spacecraft detects ENAs arriving at the spacecraft from within a 90°FOV that is swept through 360° every 2 min by the spacecraft spin, which has a vector antialigned with the orbital angular momentum vector (i.e., the spin axis is normal to the orbital plane) [*Moore et al.*, 2000]. The general direction of the cusp can be covered by a part of the 360° sweep [e.g., *Taguchi et al.*, 2005]. Figure 1 shows an example of the near-noon orbit of IMAGE (1800–1900 UT on 27 March 2001), from which the outward FOV of the LENA imager can point in the general direction of the cusp.

[9] Figures 1a and 1b represent the orbit in the $X_{GSM}Z_{GSM}$-plane and the $X_{GSM}Y_{GSM}$-plane, respectively. IMAGE was located near (X_{GSM}, Z_{GSM}) = (3–3.5 R_E, 6–7 R_E) in the near-noon sector (Y_{GSM} ~ 0) during this interval. The dotted curve in Figure 1a shows the radial distance of 8 R_E from the center of the Earth. This radius of 8 R_E is thought to lie somewhere between the satellite position and the magnetopause, and the "screen" at this radius is useful in monitoring the source ions for the LENA cusp signal [e.g., *Taguchi et al.*, 2005]. The region surrounded by diamonds in Figure 1b shows a part of the screen which consists of the seventeen 8° sectors of the spin angle (=136° out of 360°) and the 90° sectors along the polar direction of the LENA

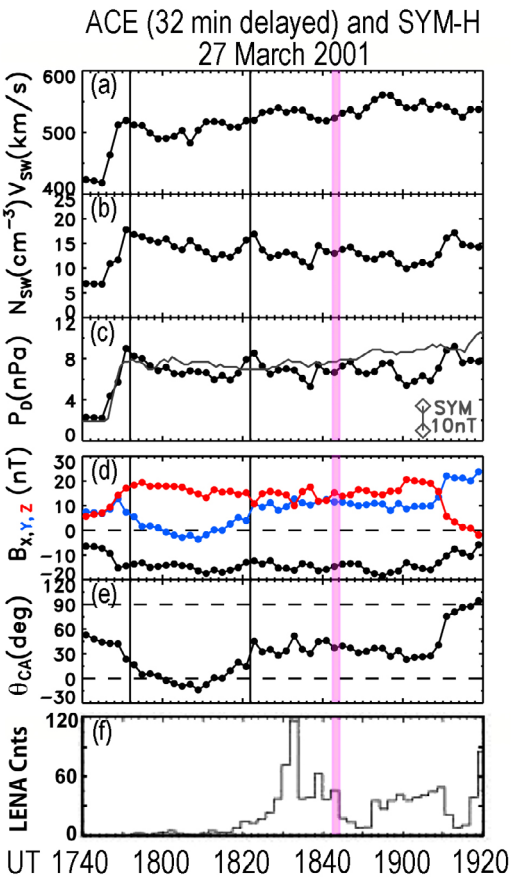

Figure 2. Comparison between the solar wind data obtained by ACE spacecraft and IMAGE/LENA hydrogen counts during 1740–1920 UT on 27 March 2001. This period includes the interval of the IMAGE orbit shown in Figure 1. The data from ACE, located ~220 R_E upstream in the solar wind, were delayed by 32 min. The two vertical lines demarcate the interval in which the magnitude of the IMF clock angle θ_{CA} was less than 20°. The purple line indicates the time for an example of LENA snapshots, which will be shown in Figure 3.

imager. We defined the sunward boundary of this FOV as three sectors away from the solar direction, and we took the nightside boundary of the FOV as the sector whose line of sight (LOS) intersects the screen at the position nearest $X_{GSM} = 0$.

[10] In this example, the FOV spans the range from $X_{GSM} \sim 4\ R_E$ to $X_{GSM} \sim 0$ on the screen. The dimension of the FOV in the Y_{GSM}-direction (i.e., the azimuthal direction) is relatively small. The distorted shape simply reflects that the middle part of the screen (i.e., near $X_{GSM} \sim 3\ R_E$) is closer to the location of the spacecraft than the parts with smaller or larger values of X_{GSM}.

[11] Since the dimension of the FOV in the azimuthal direction is relatively small, the LENA imager can sometimes miss the cusp ion injection. In other words, the right direction of the FOV relative to the cusp injection region might be a controlling factor in the ENA detection. The importance of this factor has been pointed out by *Murata et al.* [2007] and *Taguchi et al.* [2009a]. *Taguchi et al.* [2009a] have shown that when pointing in the general direction of the cusp the FOV of the LENA imager can miss the cusp signal when IMF B_Z becomes strongly negative. A similar possibility should be considered for a positive B_Z case, which is dealt with in this paper.

[12] Figure 2 shows an example of the variations in the LENA counts (27 March 2001 event) that includes a period during which the FOV of the LENA imager was in the general direction of the cusp and might have missed the cusp signal. Variations in the total LENA counts within this FOV during 1740–1920 UT are plotted with ACE solar wind data. The solar wind parameters (Figures 2a–2e) were shifted by 32 min by relating the ACE detection of an interplanetary shock at 1715 UT with a sudden commencement in the H-component of the SYM index (gray line in Figure 2c) at 1747 UT, as was done in the study by *Taguchi et al.* [2006]. Note that there are typographical errors in the descriptions of these two reference times in the study by *Taguchi et al.* [2006].

[13] The ACE data show that the solar wind speed was 500–550 km s^{-1} during most of the plotted interval following the sharp increase at 1747 UT (Figure 2a). At that time, the solar wind number density also increased to exhibit relatively high values; i.e., 10–18 cm^{-3} (Figure 2b). Because of these high number densities, the solar wind dynamic pressure (Figure 2c) was also moderately high (>6 nPa) during most of the interval.

[14] A high solar wind density causes a large ion injection flux, and in turn a larger ion injection flux creates stronger ENA signals. This implies that the LENA counts within the FOV in the direction of the cusp should be high when the solar wind density is high. Figure 2f shows the variations of the LENA counts in the general direction of the cusp. We defined the FOV by a method similar to the method applied in Figure 1b, so the FOV consists of 17 ± 1 spin-angle sectors; that is, the number of sectors is approximately constant throughout the plotted interval. It was not until ~1820 UT that the LENA counts increased, despite the fact that the solar wind density (Figure 2b), which is a controlling factor of the LENA count, had already increased at around 1750 UT and continued to exhibit a relatively high value.

[15] What is noticeable during 1750–1820 UT is the small IMF B_Y (blue line in Figure 2d). The B_Z (red line in Figure 2d) was relatively constant at ~20 nT during this interval, and the IMF clock angle θ_{CA} (Figure 2e) was also small. The two vertical lines demarcate the interval in which $|\theta_{CA}|$ (Figure 2e) was less than 20°. A small $|\theta_{CA}|$ appears to be related to very low LENA counts.

[16] Such a small $|\theta_{CA}|$ would be favorable for reconnection poleward of the cusp. In fact, *Taguchi et al.* [2006] have analyzed convection data obtained from the dayside ionosphere by SuperDARN radars on that day, and they have shown that sunward flow in the dayside polar cap, which is driven by reconnection poleward of the cusp, was present during 1750–1820 UT. This indicates that ion injection from the reconnection site should be present and that ENA emissions should be produced by the ion injection. The reason that the LENA imager did not substantially detect the ENAs during 1750–1820 UT is that its FOV was not in the right direction relative to the ENA emissions.

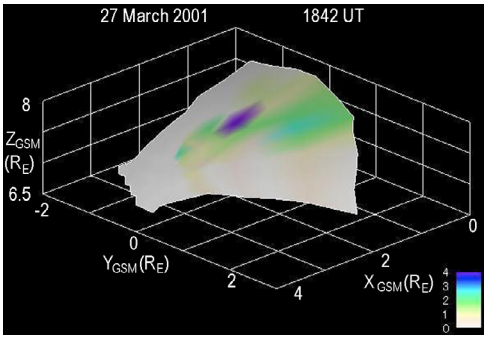

Figure 3. Example of LENA snapshots observed in the direction of the very high latitude magnetopause for northward IMF at 1842 UT on 27 March 2001. Hydrogen counts are plotted on the sphere with a radius of 8 R_E.

[17] The FOV of the LENA imager during 1750–1820 UT is similar to that shown in Figure 1b and covers the noon (Y_{GSM} = 0) meridian. This indicates that the significant part of the cusp ion injection for θ_{CA} near zero (during 1750–1820 UT) occurs somewhat apart from the Y_{GSM} = 0 meridian. This is different from the predictions by the models of the magnetic fields of the magnetosphere and magnetosheath [*Luhmann et al.*, 1984], in which reconnection occurs near the Y = 0 meridian for θ_{CA} ~ 0°. Our statistical analysis shows that the cusp injection tends to occur near the Y = 0 meridian more frequently for θ_{CA} ~ 30° than for θ_{CA} near zero.

[18] At around 1820 UT θ_{CA} increased, and then LENA started to detect the ENAs (Figure 2f). LENA continued to observe the ENAs during positive IMF B_Z. Figure 3 shows an example of the LENA snapshots that was obtained at 1842 UT (purple line in Figure 2). The background-corrected hydrogen count rate for each line of sight (LOS) is plotted on the screen. The purple or greenish colored regions represent the emission in the direction of the cusp. The maximum emission is identified at (X_{GSM}, Y_{GSM}, Z_{GSM}) = (1.4, −0.4, 7.9) R_E. The total count within the defined FOV is 46 counts (Figure 2f). This snapshot was obtained after the period of very small θ_{CA}. Both B_Z and B_Y maintained a large value of greater than 10 nT (Figure 2d), and θ_{CA} was 37° at 1842 UT (Figure 2e).

3. Analysis

3.1. LENA Events for Northward IMF

[19] We have shown in section 2 that not only LENA events with significant counts but also those with very low counts are important for understanding the characteristics of the location of the cusp injection region. This is because the latter group of events may provide information to indicate that the ion injection occurred outside the FOV of the LENA imager. We searched for LENA emission events, including very low count events, from the period when IMAGE was at high altitude and was looking in the general direction of the cusp, somewhat from the sunward side, which is suitable for monitoring cusp ion injection. This period was defined as those intervals during which IMAGE was located at Z_{GSM} > 5 R_E and X_{GSM} > 2 R_E during the noon to midnight passes of March and April in 2001.

[20] We then examined ACE solar wind data (2 min average) obtained for the periods from 90 min before the start of each defined interval to 20 min before the end, and we took periods of time (>10 min) during which both B_Y and B_Z remained positive with $(B_Y^2 + B_Z^2)^{1/2}$ greater than 5 nT. As was stated in the Introduction, the interval of negative B_Y was not included in this study. These conditions yielded 298 min from four days of two months; i.e., 27, 28, and 31 March and 28 April in 2001.

[21] The longest period satisfying the above conditions was 1750–1914 UT on 27 March 2001. This period is included in the plotted interval of Figure 2. At the beginning of this period (i.e., 1750 UT) IMAGE was located at (X_{GSM}, Y_{GSM}, Z_{GSM}) ~ (2.9, −0.1, 7.1) R_E, and the corresponding IMF (B_Y, B_Z) was (7.4 nT, 17.1 nT) (shown in Figure 2d). Naturally, these values satisfy the requirements of the orbit and the IMF. Although the IMAGE position and IMF condition at earlier times (i.e., 1740–1748 UT) also meet the criteria, this interval was not included in the event because the LENA counts were zero (Figure 2f).

[22] We then took the position of the maximum count within the defined area of the screen; i.e., the position (X_{GSM}, Y_{GSM}, Z_{GSM}). We also summed the counts from 36 (=12 × 3) bins around the bin of maximum count. The 36 bins span three consecutive spin sectors, with the bin of maximum count within the middle one. The maximum count is denoted by C. Taking into account the solar wind time lag (e.g., 32 min for the 27 March 2001 event), we allocated the corresponding (θ_{CA}, N_{SW}) data to C and location data. For example, (C, X_{GSM}, Y_{GSM}, Z_{GSM}, θ_{CA}, N_{SW}) for the image at 1842 UT (Figure 3) was (26, 1.4, −0.4, 7.9, 37, 13) in conventional units.

[23] For all images taken over the four days, we determined the solar wind propagation time from the position of the ACE spacecraft to the Earth. This was based upon a comparison of the nearest sharp increase in the SYM-H index with a similar variation in the dynamic pressure observed by ACE, as was done in Figure 2. Several previous studies have shown that the determination of the propagation time from such a comparison serves well for LENA data analyses [e.g., *Taguchi et al.*, 2004a, 2006; *Murata et al.*, 2007; *Hosokawa et al.*, 2008].

[24] Figure 4 shows another example of a LENA image from our data set. This image was obtained at 0536 UT on 28 April 2001. The plot format of this figure is the same as that of Figure 3. The count of this event is generally lower than the count of the event in Figure 3, and the image has a somewhat spotty distribution. However, it is clear that the lowest part of the distribution is relatively strong. The maximum count (purple color) is located at (X_{GSM}, Y_{GSM}, Z_{GSM}) = (4.0, −1.4, 6.8) R_E.

[25] For this event, we determined the time lag from ACE to IMAGE/LENA as 26 min. This lag agrees with the time deduced by *Suzuki et al.* [2008], who analyzed the FUV and LENA data obtained before 0536 UT on the same day. For the solar wind data, refer to Figure 2 in the paper by *Suzuki et al.* [2008]. The sextuple (C, X_{GSM}, Y_{GSM}, Z_{GSM}, θ_{CA}, N_{SW}) for this event is (13, 4.0, −1.4, 6.8, 55, 9) in conventional units. Note that the FOV of this image covers a larger prenoon (negative Y_{GSM}) region than does that of the image shown in Figure 3. As will be shown below, the emissions

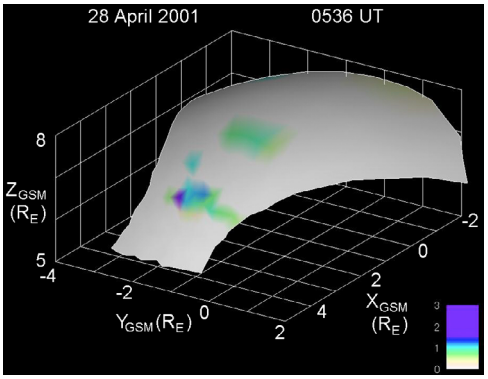

Figure 4. Example of LENA snapshots in a similar format to Figure 3. This was observed at 0536 UT on 28 April 2001. The FOV of this snapshot covers a larger prenoon (negative Y_{GSM}) region than does that of the snapshot shown in Figure 3.

depicted by the two images in Figures 3 and 4 fall into two different groups in terms of the occurrence distribution.

3.2. Method of Statistical Analysis

[26] As was shown in section 2, very small LENA counts during high solar wind densities suggest that the ion injection is present outside the polar angle range of the LENA instrument. However, when dealing with those LENA events, particularly the events obtained during moderate solar wind densities, we cannot determine unambiguously whether the observed very low count reflects this situation or simply that the emitted ENA flux is too weak to detect substantially, despite the fact that the ion injection actually occurs within the FOV. So that we can make this determination in a practical manner, we introduce the concept of effective count:

$$C_{EFF} = C \times (20/N_{SW}), \tag{1}$$

where the unit of N_{SW} is cm^{-3}. For example, when C is 10 counts for N_{SW} of 30 cm^{-3}, the effective count C_{EFF} is reduced to less than 10, whereas C_{EFF} remains greater than 10 counts for $N_{SW} < 20$ cm^{-3}. We examined how often $C_{EFF} \geq 10$ occurs for a given condition; the occurrence frequency of $C_{EFF} \geq 10$ was defined as follows:

$$R_{ij} = N_{ij}(C_{EFF} \geq 10)/N_{ij}(C_{EFF} > 0) \tag{2}$$

where N_{ij} ($C_{EFF} \geq 10$) is the number of LENA images with $C_{EFF} \geq 10$ counts under the condition that the subscripts i and j represent θ_{CA} and X_{GSM} or Y_{GSM}, while N_{ij} ($C_{EFF} > 0$) is the total number of images except for those with $C_{EFF} = C = 0$ under the same condition.

[27] Evidently, the choice of a factor of 20 in equation (1) and of a threshold value of 10 in equation (2) affects the occurrence frequency R_{ij}. For example, as the factor increases (or decreases) from 20, the occurrence frequency R_{ij} becomes large (or small) because the number of events with $C_{EFF} \geq 10$ increases (or decreases). This kind of change in R_{ij}, however, will not affect our conclusion, because our purpose is simply to identify situations in which R_{ij} is relatively high or low.

4. Results

[28] Figure 5a shows R_{ij} for i = θ_{CA} and j = X_{GSM}, while Figure 5b shows R_{ij} for i = θ_{CA} and j = Y_{GSM}. The horizontal axis of each figure represents θ_{CA} from 0° to 90°. This range means that both B_Y and B_Z are positive. The ranges of X_{GSM} (Figure 5a) and Y_{GSM} (Figure 5b) are from 0 to 6 R_E and from −3 R_E to 2 R_E, respectively. We calculated R_{ij} for each cell consisting of an X_{GSM} (or Y_{GSM}) window of 1 R_E and a θ_{CA} window of 20°. We used a moving average in which these windows are moved by 0.2 R_E and 4°, respectively; thus, a pixel of the plot is a rectangle with sides of 0.2 R_E and 4°. We assigned the value of R_{ij} to the pixel in the middle of 25 pixels composing a 1 R_E × 20° cell.

[29] In Figures 5a and 5b, a yellowish or reddish color indicates occurrence frequencies of greater than 50%, while a greenish or bluish color indicates that R_{ij} is less than 50%. The white dashed curves crudely demarcate the boundary between those two regions. Relatively high occurrence frequencies are present in Figure 5a over a wide region of X_{GSM} for θ_{CA} from ~20° to ~50° (on the left side of the vertical segment of the white dashed line). However, as θ_{CA} increases from ~50°, occurrence frequencies become low

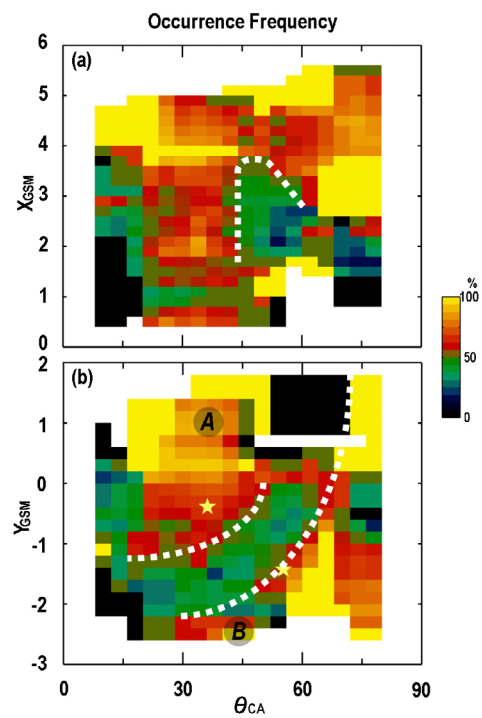

Figure 5. Occurrence frequency of the LENA cusp signals (a) in terms of the IMF clock angle (θ_{CA}) and X_{GSM} and (b) in terms of θ_{CA} and Y_{GSM}. A yellowish or reddish color indicates that occurrence frequencies are greater than 50%, while a greenish or bluish color shows the occurrence frequency of less than 50%. The white dashed curves crudely demarcate the boundary between those two regions. The two stars in Figure 5b represent the positions corresponding to the events shown in Figures 3 and 4.

roughly for $X_{GSM} < 3\ R_E$, while remaining high for relatively large X_{GSM}.

[30] It is evident in Figure 5b that relatively high occurrence frequencies are present in two separate regions. One region is labeled A and occurs in the left upper quadrant in Figure 5b, while the other is labeled B. Whereas region A corresponds to θ_{CA} of less than ~50°, region B corresponds to θ_{CA} between ~30° and ~80°. In region A the star, whose (Y_{GSM}, θ_{CA}) are (−0.4 R_E, 37°), represents the event shown in Figure 3. The event shown in Figure 4, whose (Y_{GSM}, θ_{CA}) are (−1.4 R_E, 55°), is marked by the star in region *B*. We know from this distribution that the events shown in Figures 3 and 4 fall into two different categories.

[31] We also know from this distribution that when θ_{CA} is between ~30° and ~50°, high frequencies occur in a manner of azimuthal separation. This means that cusp ion injection tends to occur in two azimuthally separated regions (in the postnoon and prenoon sectors) for those clock angles; i.e., for $B_Y > 0$ and $B_Z > 0$. This is consistent with the result obtained by *Bobra et al.* [2004].

[32] Region A tends to exhibit higher frequencies in positive Y_{GSM} (yellowish color) than in negative Y_{GSM} (reddish color). This positive Y_{GSM} preference for positive θ_{CA} is consistent with the location of antiparallel reconnection poleward of the cusp [e.g., *Luhmann et al.*, 1984], suggesting that the source of the ions for region A is caused by cusp reconnection. We can see in Figure 5a that for the clock angles of region A (i.e., from ~20° to ~50°) the region of ion injection extends tailward to small X_{GSM}. This also suggests that the source of the ions for region A is caused by cusp reconnection.

[33] On the smaller θ_{CA} side of region A (Figure 5b), the occurrence frequency is less than 50% near $Y_{GSM} = 0$ (greenish color). When we consider that the source of the ion injection for region A is cusp reconnection, this relatively low frequency near $Y_{GSM} = 0$ is somewhat puzzling. However, a similar tendency can be seen in the result obtained by *Frey et al.* [2002]. Using statistical analyses of the cusp proton aurora spot observed by IMAGE/FUV for northward IMF, *Frey et al.* [2002] have shown that the proton spots obtained near 1200 MLT, which corresponds to the $Y_{GSM} = 0$ meridian, tend to occur more often during positive IMF B_Y; i.e., for positive θ_{CA}.

5. Discussion

[34] We have suggested in the above section that when θ_{CA} is between ~30° and ~60° (Figure 5b) the ion injection tends to occur in the negative Y_{GSM} region, which is away from the injection caused by cusp reconnection. This negative Y_{GSM} region corresponds to the prenoon sector in the high-latitude ionosphere. Ion injection in the prenoon sector during those clock angles (i.e., $B_Y > 0$ and $B_Z > 0$) is consistent with the finding of *Bobra et al.* [2004] that the cusp proton aurora occurs in the unanticipated prenoon sector of the high-latitude ionosphere for $B_Y > 0$. We can see in Figure 5a that for θ_{CA} of roughly 30°–60° the occurrence frequency is continuously high at relatively large X_{GSM} (i.e., at lower latitudes), suggesting that the source of the ion injection is dayside reconnection and that the proton aurora in the unanticipated sector [*Bobra et al.*, 2004] is due to dayside reconnection.

[35] This is supported by the distribution in Figure 5b, which shows that region B, including this negative Y_{GSM} part, occurs over a wider extent, spanning both prenoon and postnoon sectors, when θ_{CA} becomes large. In response to such a relatively large θ_{CA} (i.e., the $|B_Y| > B_Z > 0$ condition), *Reiff and Burch* [1985] proposed a conceptual model in which reconnection occurs on the dayside magnetopause, despite the fact that B_Z is positive. The ionospheric feature that corresponds to this situation is standard convection, not the reversed convection typical of purely northward IMF, although the near-noon part of the standard convection is strongly controlled by IMF B_Y.

[36] Based on a statistical analysis of the electric field data from the high-latitude ionosphere during positive B_Z, *Taguchi and Hoffman* [1996] have shown that the occurrence frequency of the standard convection becomes high as $|\theta_{CA}|$ increases from 45° and that when $|\theta_{CA}|$ is between 75° and 90° the standard convection predominantly occurs in the dayside high-latitude ionosphere. The cusp field-aligned current distribution, which is associated with the dayside convection near noon, also exhibits a standard B_Y-dependent two-sheet pattern when $|\theta_{CA}|$ is between 45° and 90° as well as for larger $|\theta_{CA}|$ [*Taguchi et al.*, 1993]. These findings are consistent with the suggestion that the source for region *B* is ion injection caused by dayside reconnection and that the proton aurora in the unanticipated sector [*Bobra et al.*, 2004] is due to dayside reconnection.

[37] *Bobra et al.* [2004] show in their Figure 3 that most of the prenoon events during positive B_Y occur between 1000 MLT and 1200 MLT. To determine if these MLT regions are consistent with our region B (Figure 5b), we consider the mapping of magnetic field lines from the magnetosphere to the ionosphere. We assume a simple convergence of the Earth's magnetic field lines to the ionosphere from the radial distance of 8 R_E [e.g., *Lyons*, 1980]. The convergence factor based on magnetic flux conservation is the square root of the ratio between the magnetic field magnitudes at those two heights, $(B_M/B_I)^{1/2}$, where B_M and B_I represent the magnitudes of the magnetic field at the geocentric distance of 8 R_E and at ionospheric height, respectively. The azimuthal distance between two points, ΔY_{GSM}, on the sphere of radius 8 R_E was mapped to the distance $\Delta Y_{GSM}\ (B_M/B_I)^{1/2}$ at ionospheric height.

[38] B_M is typically 100 nT [e.g., *Paschmann et al.*, 1976; *Russell et al.*, 1998; *Fuselier et al.*, 2000], and B_I is roughly 50,000 nT at an altitude of 110 km. For example, $\Delta Y_{GSM} = 2\ R_E$ at a distance of 8 R_E would be mapped to a distance of approximately 570 km at an altitude of 110 km. When we assume that this azimuthal distance is along the magnetic latitude of 75°, a distance of 570 km corresponds to approximately 1.3 h in MLT. By making a further assumption that $Y_{GSM} = 0$ is mapped to 1200 MLT, we can infer that the points on $Y_{GSM} = -2\ R_E$, which represent region B in Figure 5, are mapped to somewhere between 1000 and 1100 MLT. These MLTs are consistent with the location of the prenoon aurora during positive B_Y according to *Bobra et al.* [2004].

[39] We have interpreted the results obtained in Figures 5a and 5b as effects from both reconnection poleward of the cusp and dayside reconnection. There are several studies that have given evidence for this kind of coexistence [e.g., *Weiss et al.*, 1995; *Wing et al.*, 2001; *Sandholt et al.*, 1998].

However, those reports show that the coexistence occurs primarily when $|B_Y| > |B_Z|$. In contrast, our Figure 5 shows that the coexistence can occur even for $|B_Z| \geq |B_Y|$.

[40] Using data obtained from the all-sky imaging photometer onboard an aircraft, *Weiss et al.* [1995] showed that zonally elongated fingers of auroral emission appear in the cusp for $|B_Y| > |B_Z|$. They explained this phenomenon in terms of the coexistence of dayside reconnection with reconnection poleward of the cusp. *Wing et al.* [2001] have analyzed data from low-altitude spacecraft and have shown that ion precipitation features created through the coexistence of the two types of reconnection can be identified even for small negative B_Z and large $|B_Y|$. By examining data from ground-based optical observations, *Sandholt et al.* [1998] showed that two types of aurora are simultaneously present in the cusp at times of $|B_Y| > |B_Z|$. Sandholt et al. attributed the two types of aurora to the coexistence of dayside reconnection with reconnection poleward of the cusp.

[41] Since region B represents a situation in which the IMF has a northward component, dayside reconnection for region B does not satisfy the antiparallel geometry of the IMF and the Earth's magnetic field. Reconnection that occurs in such geometries, with field lines of small shear angles, is referred to as component reconnection. Evidence of component reconnection for positive IMF B_Z has been provided by several studies based on in situ observations [e.g., *Onsager and Fuselier*, 1994; *Fuselier et al.*, 1997, 2000; *Chandler et al.*, 1999; *Trattner et al.*, 2004].

[42] We note that our interpretation of the phenomena for IMF $B_Y > 0$ does not require that component reconnection for positive IMF B_Z favor IMF $B_Y > 0$ rather than IMF $B_Y < 0$. We infer that component reconnection for both signs of B_Y can occur equally and that the degree of the prenoon-postnoon asymmetry of ion injection may be different between the cases. In other words, dayside reconnection (i.e., component reconnection) for IMF $B_Z > 0$ and IMF $B_Y < 0$ can cause ion injection on the northern postnoon side, but this postnoon region may be more confined to near-noon (e.g., 1200–1230 MLT in Figure 3 of *Bobra et al.* [2004]) compared to the prenoon events with positive B_Y (e.g., events between 1000 and 1200 MLT). If this kind of asymmetry actually exists, the result of *Bobra et al.* [2004] for IMF $B_Y < 0$ would also be explained in terms of reconnection.

[43] We searched for a period of LENA observation that occurred during negative B_Y while requiring $B_Z > 0$ and $(B_Y^2 + B_Z^2)^{1/2} > 5$ nT for the period of the IMAGE near-noon passes. Few intervals satisfied these conditions. The manner in which the present result can actually be related to a situation with $B_Y < 0$ and $B_Z > 0$ should be examined with a different approach.

6. Conclusions

[44] We have examined the occurrence of the IMAGE/LENA cusp signal in terms of its arrival direction and the IMF clock angle in order to identify the characteristics of the ion injection for positive IMF B_Z. Results of statistical analyses show that the occurrence frequency is high on the postnoon side when the clock angle is between ~20° and ~50°. This is ascribed to ion injection caused by cusp reconnection typical of $B_Y > 0$ and $B_Z > 0$. Our results also show that there is another situation of high occurrence frequency, which can be identified with clock angles of ~30° to ~80°. When the clock angle is relatively large (60°–80°), high occurrence frequencies are present at relatively low latitudes over a wide extent spanning both prenoon and postnoon sectors, suggesting that the ion injection is caused by reconnection on the dayside magnetopause. The postnoon side boundary of this region shifts toward the prenoon as the clock angle decreases. When the clock angles are less than ~50°, this region occurs well inside the prenoon sector, suggesting that dayside reconnection occurs in the prenoon region azimuthally separated from the region ascribed to cusp reconnection. This can explain the report by *Bobra et al.* [2004] that the proton aurora brightening occurs in the unanticipated prenoon sector of the high-latitude ionosphere for $B_Y > 0$ and $B_Z > 0$.

[45] **Acknowledgments.** This work was supported in part by Grant-in-Aid for Scientific Research (B) 22340143 under Japan Society for the Promotion of Science. M. Abe would like to thank K. Hosokawa for valuable discussion. ACE magnetic field and plasma data were provided by N. Ness and D. McComas through the NASA CDAWeb.

[46] Masaki Fujimoto thanks the reviewers for their assistance in evaluating this paper.

References

Avanov, L., V. Smirnov, J. Waite Jr., S. Fuselier, and O. Vaisberg (2001), High-latitude magnetic reconnection in sub-Alfvénic flow: Interball tail observations on May 29, 1996, *J. Geophys. Res.*, *106*(A12), 29,491–29,502, doi:10.1029/2000JA000460.

Bobra, M. G., S. M. Petrinec, S. A. Fuselier, E. S. Claflin, and H. E. Spence (2004), On the solar wind control of cusp aurora during northward IMF, *Geophys. Res. Lett.*, *31*, L04805, doi:10.1029/2003GL018417.

Burke, W., M. Kelley, R. Sagalyn, M. Smiddy, and S. Lai (1979), Polar cap electric field structures with a northward interplanetary magnetic field, *Geophys. Res. Lett.*, *6*(1), 21–24, doi:10.1029/GL006i001p00021.

Chandler, M., S. Fuselier, M. Lockwood, and T. Moore (1999), Evidence of component merging equatorward of the cusp, *J. Geophys. Res.*, *104*(A10), 22,623–22,633, doi:10.1029/1999JA900175.

Collier, M. R., et al. (2001a), Observations of neutral atoms from the solar wind, *J. Geophys. Res.*, *106*(A11), 24,893–24,906, doi:10.1029/2000JA000382.

Collier, M. R., et al. (2001b), LENA observations on March 31, 2001: Magnetosheath remote sensing, *Eos Trans. AGU*, *82*(47), Fall Meet. Suppl., Abstract SM41C-05.

Collier, M. R., T. E. Moore, M.-C. Fok, B. Pilkerton, and H. Khan (2005), Low-energy neutral atom signatures of magnetopause motion in response to southward B_Z, *J. Geophys. Res.*, *110*, A02102, doi:10.1029/2004JA010626.

Collier, M. R., D. G. Sibeck, T. E. Cravens, I. P. Robertson, and N. Omidi (2010), Astrophysics noise: A space weather signal, *Eos Trans. AGU*, *91*(24), 213, doi:10.1029/2010EO240001.

Crooker, N. U. (1979), Dayside merging and cusp geometry, *J. Geophys. Res.*, *84*(A3), 951–959, doi:10.1029/JA084iA03p00951.

Eriksson, S., J. W. Bonnell, L. G. Blomberg, R. E. Ergun, G. T. Marklund, and C. W. Carlson (2002), Lobe cell convection and field-aligned currents poleward of the region 1 current system, *J. Geophys. Res.*, *107*(A8), 1185, doi:10.1029/2001JA005041.

Fok, M.-C., et al. (2003), Global ENA IMAGE simulations, *Space Sci. Rev.*, *109*, 77–103, doi:10.1023/B:SPAC.0000007514.56380.fd.

Frey, H. U. (2007), Localized aurora beyond the auroral oval, *Rev. Geophys.*, *45*, RG1003, doi:10.1029/2005RG000174.

Frey, H. U., S. B. Mende, T. J. Immel, S. A. Fuselier, E. S. Claflin, J. Gérard, and B. Hubert (2002), Proton aurora in the cusp, *J. Geophys. Res.*, *107*(A7), 1091, doi:10.1029/2001JA900161.

Fuselier, S., B. Anderson, and T. Onsager (1997), Electron and ion signatures of field line topology at the low-shear magnetopause, *J. Geophys. Res.*, *102*(A3), 4847–4863, doi:10.1029/96JA03635.

Fuselier, S. A., K. J. Trattner, and S. M. Petrinec (2000), Cusp observations of high- and low-latitude reconnection for northward interplanetary mag-

netic field, *J. Geophys. Res.*, *105*(A1), 253–266, doi:10.1029/1999JA900422.

Fuselier, S. A., et al. (2010), Energetic neutral atoms from the Earth's subsolar magnetopause, *Geophys. Res. Lett.*, *37*, L13101, doi:10.1029/2010GL044140.

Heelis, R., P. Reiff, J. Winningham, and W. Hanson (1986), Ionospheric convection signatures observed by DE 2 during northward interplanetary magnetic field, *J. Geophys. Res.*, *91*(A5), 5817–5830, doi:10.1029/JA091iA05p05817.

Hosokawa, K., S. Taguchi, S. Suzuki, M. R. Collier, T. E. Moore, and M. F. Thomsen (2008), Estimation of magnetopause motion from low-energy neutral atom emission, *J. Geophys. Res.*, *113*, A10205, doi:10.1029/2008JA013124.

Kessel, R. L., S.-H. Chen, J. L. Green, S. F. Fung, S. A. Boardsen, L. C. Tan, T. E. Eastman, J. D. Craven, and L. A. Frank (1996), Evidence of high-latitude reconnecting during northward IMF: Hawkeye observations, *Geophys. Res. Lett.*, *23*(5), 583–586, doi:10.1029/95GL03083.

Knipp, D., et al. (1993), Ionospheric convection response to slow, strong variations in a northward interplanetary magnetic field: A case study for January 14, 1988, *J. Geophys. Res.*, *98*(A11), 19,273–19,292, doi:10.1029/93JA01010.

Lavraud, B., et al. (2002), Cluster observations of the exterior cusp and its surrounding boundaries under northward IMF, *Geophys. Res. Lett.*, *29*(20), 1995, doi:10.1029/2002GL015464.

Lavraud, B., et al. (2005), High-altitude cusp flow dependence on IMF orientation: A 3-year Cluster statistical study, *J. Geophys. Res.*, *110*, A02209, doi:10.1029/2004JA010804.

Luhmann, J. G., R. J. Walker, C. T. Russell, N. U. Crooker, J. R. Spreiter, and S. S. Stahara (1984), Patterns of potential magnetic field merging sites on the dayside magnetopause, *J. Geophys. Res.*, *89*(A3), 1739–1742, doi:10.1029/JA089iA03p01739.

Lyons, L. (1980), Generation of large-scale regions of auroral currents, electric potentials, and precipitation by the divergence of the convection electric field, *J. Geophys. Res.*, *85*(A1), 17–24, doi:10.1029/JA085iA01p00017.

Maezawa, K. (1976), Magnetospheric convection induced by the positive and negative Z components of the interplanetary magnetic field: Quantitative analysis using polar cap magnetic records, *J. Geophys. Res.*, *81*(13), 2289–2303, doi:10.1029/JA081i013p02289.

Matsuoka, A., K. Tsuruda, H. Hayakawa, T. Mukai, and A. Nishida (1996), Electric field structure and ion precipitation in the polar region associated with northward interplanetary magnetic field, *J. Geophys. Res.*, *101*(A5), 10,711–10,736, doi:10.1029/95JA03557.

McComas, D. J., et al. (2009), IBEX—Interstellar Boundary Explorer, *Space Sci. Rev.*, *146*, 11–33, doi:10.1007/s11214-009-9499-4.

Mende, S. B., et al. (2000), Far ultraviolet imaging from the IMAGE spacecraft, *Space Sci. Rev.*, *91*, 243–270, doi:10.1023/A:1005271728567.

Milan, S. E., M. Lester, S. W. H. Cowley, and M. Brittnacher (2000), Dayside convection and dayside morphology during an interval of northward interplanetary magnetic field, *Ann. Geophys.*, *18*, 436–444, doi:10.1007/s00585-000-0436-9.

Moore, T. E., et al. (2000), The low-energy neutral atom imager for IMAGE, *Space Sci. Rev.*, *91*, 155–195, doi:10.1023/A:1005211509003.

Moore, T. E., et al. (2001), Low energy neutral atoms in the magnetosphere, *Geophys. Res. Lett.*, *28*(6), 1143–1146, doi:10.1029/2000GL012500.

Moore, T. E., et al. (2003), Heliosphere-geosphere interactions using low energy neutral atom imaging, *Space Sci. Rev.*, *109*, 351–371, doi:10.1023/B:SPAC.0000007524.11258.b4.

Murata, Y., S. Taguchi, K. Hosokawa, A. Nakao, M. R. Collier, T. E. Moore, N. Sato, H. Yamagishi, and A. S. Yukimatu (2007), Correlative variations of the neutral atom emission in the high-altitude cusp and the low-altitude cusp, *J. Geophys. Res.*, *112*, A11208, doi:10.1029/2007JA012404.

Onsager, T. G., and S. A. Fuselier (1994), The location of magnetopause reconnection for northward and southward interplanetary magnetic field, in *Solar System Plasmas in Space and Time*, *Geophys. Monogr. Ser.*, vol. 84, edited by J. L. Burch and J. H. Waite Jr., pp. 183–197, AGU, Washington, D. C.

Paschmann, G., G. Haerendel, N. Sckopke, H. Rosenbauer, and P. C. Hedgecock (1976), Plasma and magnetic field characteristics of the distant polar cusp near local noon: The entry layer, *J. Geophys. Res.*, *81*(16), 2883–2899, doi:10.1029/JA081i016p02883.

Petrinec, S. M., et al. (2011), Neutral atom imaging of the magnetospheric cusps, *J. Geophys. Res.*, *116*, A07203, doi:10.1029/2010JA016357.

Phan, T., et al. (2003), Simultaneous Cluster and IMAGE observations of cusp reconnection and auroral proton spot for northward IMF, *Geophys. Res. Lett.*, *30*(10), 1509, doi:10.1029/2003GL016885.

Reiff, P. (1982), Sunward convection in both polar caps, *J. Geophys. Res.*, *87*(A8), 5976–5980, doi:10.1029/JA087iA08p05976.

Reiff, P. H., and J. L. Burch (1985), IMF By-dependent plasma flow and Birkeland currents in the dayside magnetosphere: 2. A global model for northward and southward IMF, *J. Geophys. Res.*, *90*(A2), 1595–1609, doi:10.1029/JA090iA02p01595.

Russell, C. T., J. A. Fedder, S. P. Slinker, X.-W. Zhou, G. Le, J. G. Luhmann, F. R. Fenrich, M. O. Chandler, T. E. Moore, and S. A. Fuselier (1998), Entry of the Polar spacecraft into the polar cusp under northward IMF conditions, *Geophys. Res. Lett.*, *25*(15), 3015–3018, doi:10.1029/98GL00355.

Sandholt, P. E., C. J. Farrugia, J. Moen, and S. W. H. Cowley (1998), Dayside auroral configurations: Responses to southward and northward rotations of the interplanetary magnetic field, *J. Geophys. Res.*, *103*(A9), 20,279–20,295.

Suzuki, S., S. Taguchi, K. Hosokawa, M. R. Collier, T. E. Moore, H. U. Frey, and S. B. Mende (2008), Conjugate observations of ENA signals in the high-altitude cusp and proton auroral spot in the low-altitude cusp with IMAGE spacecraft, *Geophys. Res. Lett.*, *35*, L13103, doi:10.1029/2008GL034543.

Taguchi, S., and R. A. Hoffman (1996), Control parameters for polar ionospheric convection patterns during northward interplanetary magnetic field, *Geophys. Res. Lett.*, *23*, 637–640, doi:10.1029/96GL00452.

Taguchi, S., M. Sugiura, J. D. Winningham, and J. A. Slavin (1993), Characterization of the IMF B_Y-dependent field-aligned currents in the cleft region based on DE 2 observations, *J. Geophys. Res.*, *98*(A2), 1393–1407, doi:10.1029/92JA01014.

Taguchi, S., M. R. Collier, T. E. Moore, M.-C. Fok, and H. J. Singer (2004a), Response of neutral atom emissions in the low- and high-latitude magnetosheath direction to the magnetopause motion under extreme solar wind conditions, *J. Geophys. Res.*, *109*, A04208, doi:10.1029/2003JA010147.

Taguchi, S., K. Hosokawa, M. R. Collier, T. E. Moore, M.-C. Fok, A. S. Yukimatu, N. Sato, and R. A. Greenwald (2004b), Simultaneous observations of the cusp with IMAGE Low Energy Neutral Atom imager and SuperDARN radar, *Adv. Polar Upper Atmos. Res.*, *18*, 53–64.

Taguchi, S., S.-H. Chen, M. R. Collier, T. E. Moore, M.-C. Fok, K. Hosokawa, and A. Nakao (2005), Monitoring the high-altitude cusp with the Low Energy Neutral Atom imager: Simultaneous observations from IMAGE and Polar, *J. Geophys. Res.*, *110*, A12204, doi:10.1029/2005JA011075.

Taguchi, S., K. Hosokawa, A. Nakao, M. R. Collier, T. E. Moore, A. Yamazaki, N. Sato, and A. S. Yukimatu (2006), Neutral atom emission in the direction of the high-latitude magnetopause for northward IMF: Simultaneous observations from IMAGE spacecraft and SuperDARN radar, *Geophys. Res. Lett.*, *33*, L03101, doi:10.1029/2005GL025020.

Taguchi, S., K. Hosokawa, A. Nakao, M. R. Collier, T. E. Moore, N. Sato, and A. S. Yukimatu (2009a), HF radar polar patch and its relation with the cusp during B_Y-dominated IMF: Simultaneous observations at two altitudes, *J. Geophys. Res.*, *114*, A02311, doi:10.1029/2008JA013624.

Taguchi, S., S. Suzuki, K. Hosokawa, Y. Ogawa, A. S. Yukimatu, N. Sato, M. R. Collier, and T. E. Moore (2009b), Moving mesoscale plasma precipitation in the cusp, *J. Geophys. Res.*, *114*, A06211, doi:10.1029/2009JA014128.

Torr, M. R., et al. (1995), A far ultraviolet imager for the international solar-terrestrial physics mission, *Space Sci. Rev.*, *71*, 329–383, doi:10.1007/BF00751335.

Trattner, K. J., S. A. Fuselier, and S. M. Petrinec (2004), Location of the reconnection line for northward interplanetary magnetic field, *J. Geophys. Res.*, *109*, A03219, doi:10.1029/2003JA009975.

Weiss, L., P. Reiff, E. Weber, H. Carlson, M. Lockwood, and W. Peterson (1995), Flow-aligned jets in the magnetospheric cusp: Results from the Geospace Environment Modeling pilot program, *J. Geophys. Res.*, *100*(A5), 7649–7659, doi:10.1029/94JA03360.

Wing, S., P. Newell, and J. Ruohoniemi (2001), Double cusp: Model prediction and observational verification, *J. Geophys. Res.*, *106*(A11), 25,571–25,593, doi:10.1029/2000JA000402.

M. Abe and S. Taguchi, Department of Communication Engineering and Informatics, University of Electro-Communications, Tokyo 182-8585, Japan. (taguchi@ice.uec.ac.jp)

M. R. Collier and T. E. Moore, NASA Goddard Space Flight Center, Greenbelt, MD 20771, USA.